Development of Post-tensioned Laminated Glass Beam

David Antolinc [a], Darjan Grudnik [b]

a. University of Ljubljana, Faculty of Civil and Geodetic Engineering, Slovenia, david.antolinc@fgg.uni-lj.si

b. CGP d.d., Slovenia, grudnik.darjan@gmail.com

Abstract

One of the advantages of flat glass is its extremely high compressive strength, which can reach up to 1000 MPa. Because of the significantly lower glass tensile strength, the high compressive strength of the glass remains unexploited when the glass elements are loaded in bending and one side of the element experiences the tensile stresses. One of the options to increase the tensile strength of the glass is through the process of the glass fiber production. The tensile strength of glass fibers is in the range of 2500 MPa and 4500 MPa which is significantly higher in comparison to any other glass product. By combining both, flat glass sheets and glass fibers with a concept similar to conventional reinforced concrete beams we present in this paper the innovative post-tensioned beam. The beam is assembled with the series of flat glass sheets stacked together along the longitudinal axis of the beam which is oriented perpendicularly to the surfaces of the stacked glass sheets. At the bottom of the proposed glass beam cross section is a hole along the whole length of the beam for the installation of the continuous glass fiber rope which is used for the post-tensioning and to facilitate the tension stresses. Based on the numerical simulation and the preliminary experimental analysis of the individual components and their interactions we can conclude that the proposed idea present a potential for a beam completely made of glass with a high load bearing capacity. However, some limitations and guidelines for further research are also discussed.

Keywords

Laminated glass, Glass fibers, UV adhesive, EVA interlayer, post-tensioned glass beam

Article Information

- Published by Glass Performance Days, on behalf of the author(s)
- Published as part of the Glass Performance Days Conference Proceedings, June 2025
- Editors: Jan Belis, Christian Louter & Marko Mökkönen

1. Introduction

There are numerous realised examples of load bearing bending beams where glass is used as a structural material. The most common concept is to use laminated glass as thin layered shell structure without any reinforcement where its largest cross section dimension is oriented vertically. Several authors have studied and tested upgraded versions of laminated glass beams with additional reinforcement in form of stainless-steel rods and sections (Louter et al., 2012), glass or carbon fiber reinforced polymer profiles (GFRP or CFRP) (Bedon & Louter, 2019; Cagnacci et al., 2021) and glass or carbon fiber reinforcement (Louter et al., 2010). Further improvement of laminated glass beams can be achieved with prestressing or post-tensioning of reinforcements in different forms (Bedon & Louter, 2018; Martens et al., 2016). Based on the previous research provided in the literature it can be generally concluded that the addition of reinforcements in different forms have a beneficial effect on the stiffness, load bearing resistance, ductility and redundancy trough enabled post-fracture loadbearing capacity (Bedon & Louter, 2019). A thorough review of the research for reinforced and post-tensioned laminated glass beams was done by Martens et al. (2016) where more detailed information is collected. Based on the collected data from previous researches they calculated the post fracture performance as the ratio of ultimate failure load and failure initiating load among other parameters and it was found out that it can reach high values of up to 2,5 in case of post-tensioned laminated beams and 1,3 on average for all reviewed concepts. More recently an interesting and innovative posttensioning concept was developed and studied by Silvestru et al. (2024) where pre-strained iron-based shape memory alloy tendon was adhesively bonded on both longitudinal edges of the laminated glass beam. The post-tensioning process is then followed by the tendon shape memory effect triggered by the electrical resistive heating. It was proved that the force at the initial pronounced glass crack of the activated and post-tensioned beam can be up to 22% higher in comparison to the reinforced laminated glass beam without tendon activation. Additionally, it was shown that initial beam stiffness was not changed atter the activation of post-tensioning.

In the recent years the research on topic of cast glass elements have been advanced (Bristogianni et al., 2017, 2021; Dimas et al., 2022; Oikonomopoulou et al., 2018). Consequently, the idea to produce the interlocking cast glass elements and stack them together to form an arch bridge beam was studied by Aurik (Aurik, 2017; Aurik et al., 2018; Snijder et al., 2016). Along with this concept the idea to build a pot-tensioned beam composed of cast glass elements stacked together along the beam length and then post-tensioned with a tendon running through the bottom of the beam cross section and fixed at both ends was mentioned and discussed by Snijder A. et al. (2016). For both, the arch and post-tensioned cast glass beams fatal tensile stresses result from nonuniform stress distribution caused by the external load and second from a stress concentration between adjacent cast glass elements as a result of local surface irregularities or overall glass element imperfections.

To overcome these problems, we suggest to use float flat glass sheets stacked together along the longitudinal axis of the beam which is oriented perpendicularly to the surfaces of the stacked glass sheets where more details are provided in the following sections.

1.1. The idea and concept of the proposed prestressed glass beam

The main idea of the proposed and studied post-tensioned beam was to create a bending beam that is almost entirely made of glass and has the highest possible load bearing capacity. This can be at least theoretically achieved by combining the float flat glass to take over the compressive stresses and glass fiber rope in tension zone to deal with the tensile stresses. Therefore, we propose the beam assembled with the series of 70 float annealed glass sheets stacked together along the longitudinal axis of the beam which is oriented perpendicularly to the surfaces of the stacked glass sheets as shown in Figure 1. Each flat glass sheet is 80 mm wide, 120 mm high and with the thickness of 20 mm, which is forming the final glass beam geometry with the length of 1400 mm when all of the glass sheets are stacked together. There is also a hole with the diameter of 20 mm in each of the glass sheets at the bottom part of the cross section, finally forming an opening running through the bottom part of the studied beam dedicated for the installation of the glass fiber tendon with the diameter of 18 mm. Centreline of the hole is horizontally positioned at the centreline of the cross section and 30 mm from the bottom surface of the beam cross section. Four point bending beam is spanning a distance of 1 m between the supports and is loaded with two forces at the distance of 300 mm between each other.

We assume that the float glass production process provides us as smooth as possible surface without local detrimental irregularities. Furthermore, inspired by the mechanically anchored post-tensioned tendons concept studied by Louter in (Louter et al, 2013) we suggest to use the same concept to post-tension all of the stacked glass sheets together with glass fiber tendon eccentrically positioned at lower part of the beam cross-section. For the numerical modelling we propose to apply post-tensioning force of 300 kN in the glass fiber tendon which is anchored at each side of the beam trough the steel plates with the dimensions of 40 mm / 40 mm and thickness of 10 mm where post-tensioning load is transferred to the glass sheets. There are some drawbacks with the proposed post-tensioning system such as the compression stress concentrations on each side of the beam when post-tensioning load is transferred to the glass sheets elements. This problem is addressed in further sections with the numerical simulation. Another issue represents an impaired transparency of the beam because of many relatively thin glass sheets where the light is reflecting. Since the friction coefficient between adjacent smooth flat glass sheets is very low another concern rises when applying shear forces on the proposed beam. Therefore, we suggest EVA interlayer or acrylate UV glue to provide shear resistance between glass sheets. Both of them were used to prepare laminated glass specimens for shear load bearing and stiffness behaviour testing and are presented in this article in the next section.

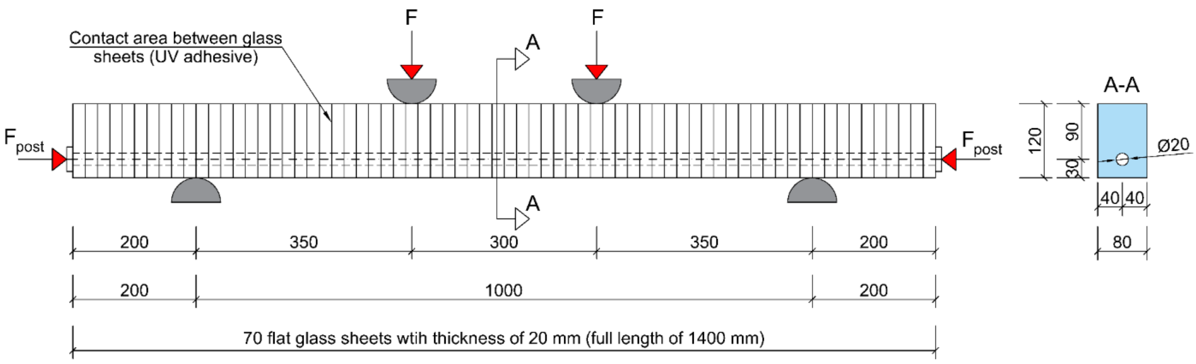

Fig. 1: Concept and geometry of proposed glass beam assembled of flat glass sheets and post-tensioned glass fiber tendon.

2. Experimental analysis of glass-interlayer interaction and glass fiber tendon

2.1. Materials

For both shear testing specimens, the standard float annealed glass sheets with the thickness of 10 mm were used. All edges of glass sheets were polished. Two types of bonding materials between glass sheets were used to observe their response under shear load. Firstly, the acrylic UV adhesive was used which is applied as a very thin (thickness of less than 0.1 mm) virtually negligible thickness of adhesive layer. This means that the adhesive layer does not provide any possibility for the compensation of irregularities on the contact surface between two glass sheets. We assumed that this will not be a problem since we have used perfectly flat and smooth float glass and therefore, we avoid the risk of creating local stress concentrations. According to the UV adhesive manufacturer specification the shear strength is 17 MPa (*Properties of Adhesives at a Glance*, 2017; *UV Adhesive Verfix LV 740, Technical Data*, 2017). The second interlayer material used was EVA foil with the thickness of 1.3 mm (*Strato Glass Interlayers, Data Sheets for EVA Interlayers*, 2018). The reinforcement used for post-tensioning was glass fiber tendon (Direct Roving 469P) with the linear density of 2,4 g/m, modulus of elasticity equal to 70 GPa and with the tendon diameter of 18 mm. Tensile strength of glass fiber tendon was evaluated based on the conducted tensile test presented in the sections below. Additionally, compression test on specimens bonded with the EVA interlayer and UV adhesive were conducted but were not successful due to a premature failure as we have used to soft rubber pads between glass sheets and the steel plates of the compression machine and thus, we do not present these results here in this article.

2.2. Shear test with results discussion

To enhance the numerical model of the proposed post-tensioned glass beam, the information about the UV adhesive or EVA interlayer shear stiffness behaviour is needed. Therefore, we prepared one specimen for each of the studied glass to glass interaction materials with the specially designed specimens to apply in-plane shear stresses to the contact area between the glass sheets as shown in the Figure 2. The specimens are assembled with three layers of 10 mm thick and 80 mm wide annealed float glass sheets where the middle glass sheet is 60 mm longer in comparison to the adjacent 120 mm high glass sheets. The specimens are then inserted into the compression machine on two separated linear supports as shown in the Figure 3, which are supporting only the adjacent glass sheets and enabling the middle glass sheet unrestrictedly translating when loaded with the compression load above. To measure the relative displacement of the middle glass sheet in regards to the adjacent ones we placed two extensometers on each side of the specimen on prior glued aluminium plates on the edges of all glass sheets (see Figure 3).

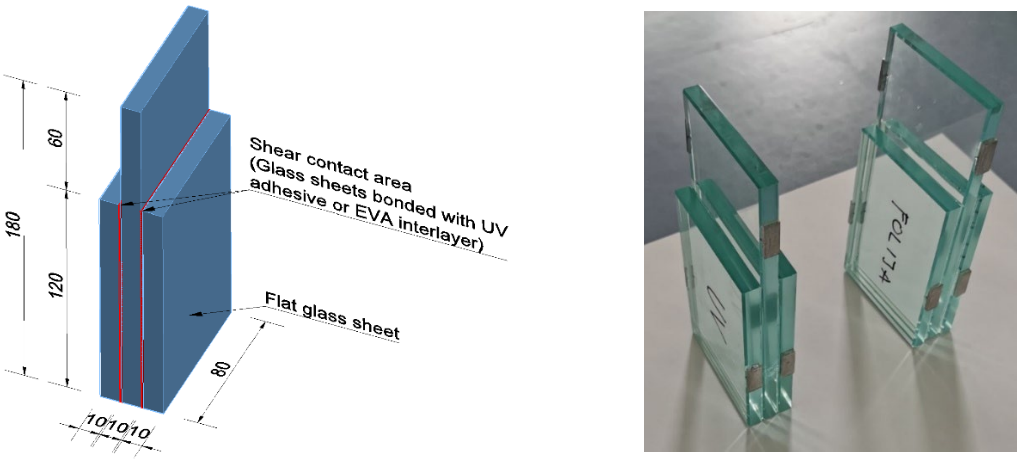

Fig. 2: Dimensions of shear testing specimens (left) and picture of the specimens (right) with attached aluminium plates for the fixation of extensometers.

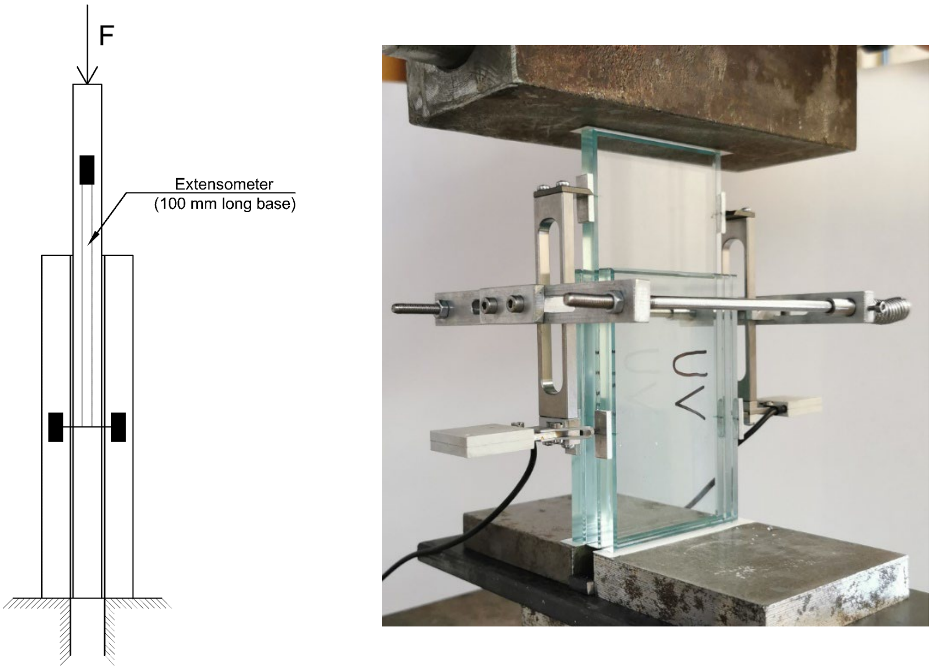

Fig. 3: Side view of the shear test setup (left) and picture of the shear test setup prepared in the compression machine before testing (right).

As a result of described shear test the shear stresses developed in contact area between glass sheets in a relationship to the corresponding relative deformation (average for both edges) can be presented like shown in the Figure 4 for both specimens. The red line represents the result for specimen with EVA interlayer whereas the blue line the result for the specimen with the UV adhesive. As expected, the specimen with the EVA interlayer exhibit more compliant shear behaviour in comparison to the specimen with the UV adhesive. Additionally, the specimen with EVA interlayer exhibits nonlinear behaviour, whereas the specimen with UV adhesive behaves linear up to the failure of the middle glass sheet. The failure of the specimens occurred in the glass sheets as shown in the Figure 5 as a result of compression contact stresses between the glass sheets and the steel plates of the testing machine and not as a result of adhesive failure between the bonded glass sheets. To achieve the contact failure between the glass sheets a modified version of shear specimen with relatively smaller contact area between the glass sheets would need to be prepared and tested. For the current study and the numerical simulation in the next chapter we choose UV adhesive as the bonding adhesive between glass sheets as it shows the superior shear stiffness behaviour in regards to the EVA interlayer. Based on the obtained data from the shear test the shear-slip stiffness of k_s = 45,1 MPa/mm was evaluated for the UV adhesive bond.

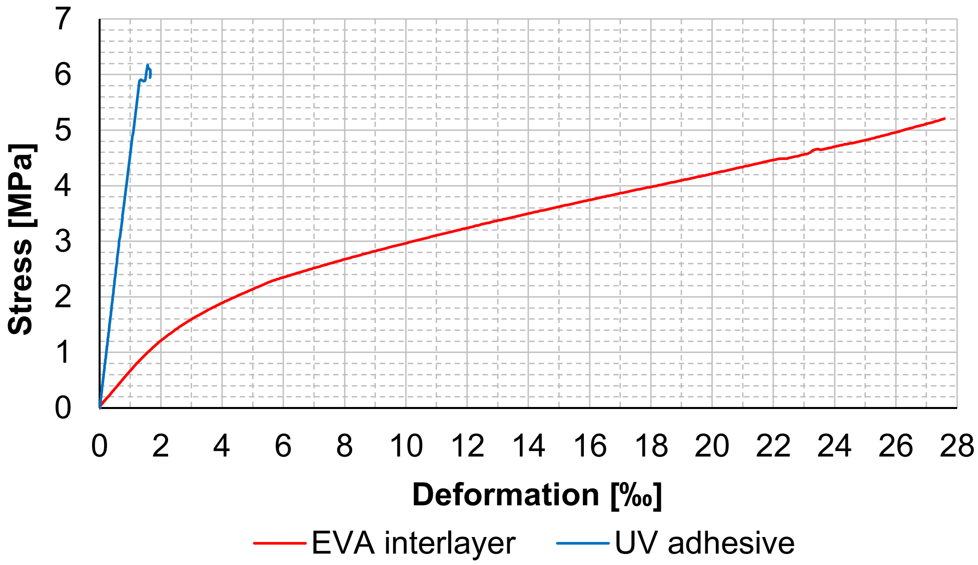

Fig. 4: Shear stress – shear deformation relationship for the specimens bonded with EVA interlayer (red line) and with UV glue (blue line).

Fig. 5: Failure mode of shear specimens bonded with EVA interlayer (left) and with UV glue (right).

2.3. Glass fiber tendon test with results discussion

Glass fibers generally exhibit relatively high tensile strength in comparison to other conventional structural materials and for purposes of the present study we considered and tested commercially available glass fiber tendon. As stated by the glass fiber producer the density and tensile load bearing capacity are 2,4 g/m and 840 N respectively. However, we decided to conduct the tensile test of the considered glass fiber tendon to check the potential downgrades in tensile strength due to the clamping system. To provide an adequate grip of the glass fiber rope specimen into the jaws of tensile testing machine we glued two aluminium plates on each side of the specimen as shown in the left Figure 6. Meanwhile there is the glass fiber rope tensile test setup shown in the right Figure 6.

Fig. 6: Prepared glass fiber rope specimen (left) and the same specimen inserted into the tensile testing machine (right).

The result of the glass fiber tendon tensile testing is shown in the Figure 7, where force in relationship to the corresponding displacement is presented. The maximum tensile force resistance was reached at 740 N which is about 12% lower than expected and declared by the producer. This is most probably the consequence of local fiber damage at the location of clamping jaws where the tensile load is transferred to the specimen. This finding is of high importance for the future design of clamping and connection detail between the glass fiber tendon and load transferring steel plates on each side of the beam to avoid premature failure of glass fibers. When considering the total cross-section area of tested glass fibers tendon equal to 0,4 mm^2 the tensile strength of 1850 MPa can be evaluated. In the left Figure 8 it is shown the initial failure of first glass fibers and in the right Figure 8 the final failure of glass fiber tendon. It is obvious that with the used type of glass fiber tendon fixation we get gradual failure of single fibers ending in final failure of glass fiber rope and that there is no strictly brittle glass fiber failure.

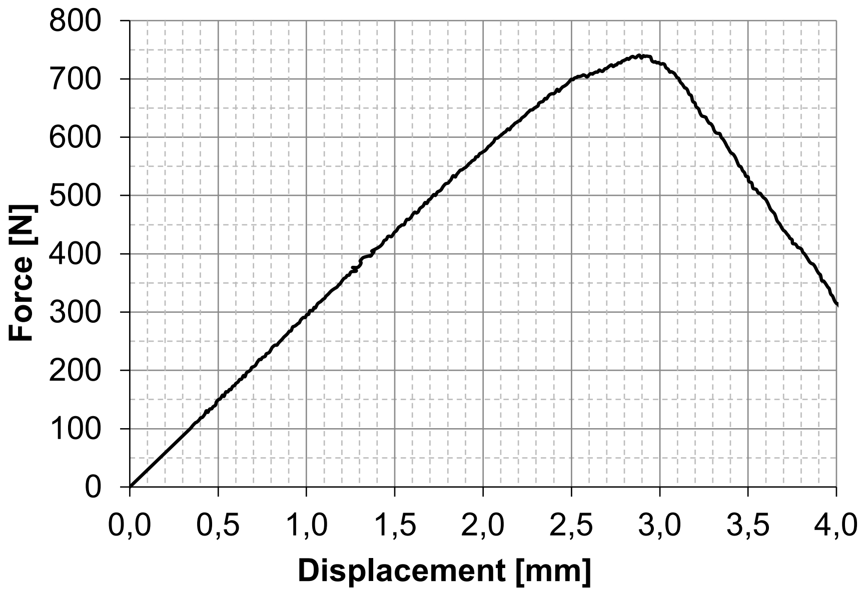

Fig. 7: The force – displacement relationship obtained from the tensile testing of glass fiber tendon.

Fig. 8: The beginning of the several glass fiber failures (left) and total glass fiber tendon failure (right).

3. Numerical modelling of small-scale postensioned glass beam

To test the feasibility and to identify mechanical problems of proposed post-tensioned laminated glass beam the numerical finite element analysis was carried out in the present research. The simulation and nurical analysis of the proposed beam was conducted with the full 3D solid finite element model prepared in ABAQUS software with the use of its standard capabilities. The geometry, dimensions and the assambly of the elments is closely following the proposed post-tensioned beam setup in the Figure 1 in the first chapter. For all three types of elements namely flat glass sheets, end steel plates and glass fibre rope the 8-node 3D solid elements (C3D8I) were used. The whole model assambly consist of 70 flat glass elements as shown in the Figure 9 and one glass fiber tendon runnig trough the hole at the bottom of the cross-section which is fixed with the end steel plates on each side of the beam to transfer the post-tensioning load to the glass elements. When preparing the numerical model special attention was given to the interaction modeling between the flat glass elements and the problematic shear stresses between them. For the glass-to-glass interaction modeling the contact properties (surface-to-surface) were defined in tangential direction with the elastic shear-slip stiffness equal to 45,1 MPa/mm for the UV adhesive as obtained by the experimental analysis of shear specimens.

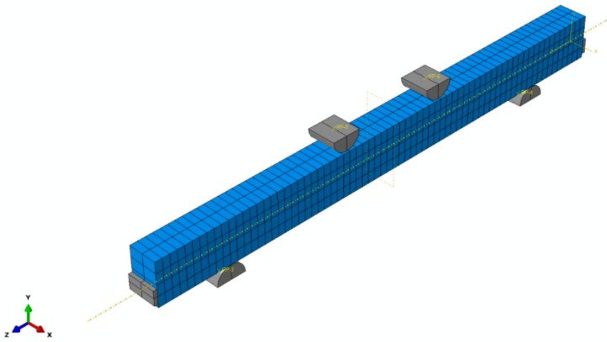

a)

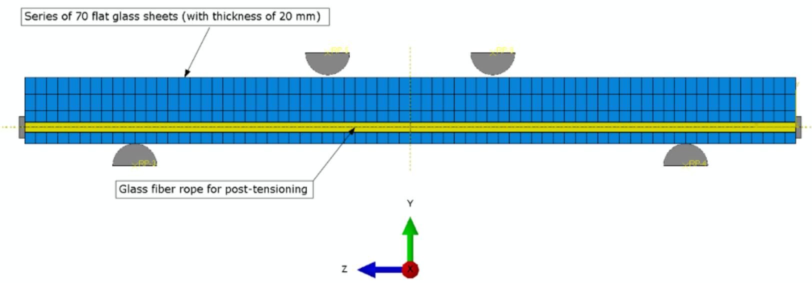

b)

Fig. 9: 3D numerical model (a) and longitudinal cross-section trough the model (b) of studied post-tensioned glass beam prepared in ABAQUS software.

The numerical analysis was performed with two consequtive loading steps. First the post-tensioning loading step was created using a “Bolt load” module to define the post tensioning load of 300 kN following by the applying this force to the glass fiber tendon cross-section. In the second loading step the displacement controlled vertical load was applied to simulate the stresses distribution, vertical deflections and the bending stiffness of the proposed beam. In the Figure 10 the normal stresses S33 along the beam axis Z are shown as a result of post-tensioning. As expected the compression stresses are present almost in the entire lower part of the beam and some tension stresses toward the upper part of the beam cross-section.

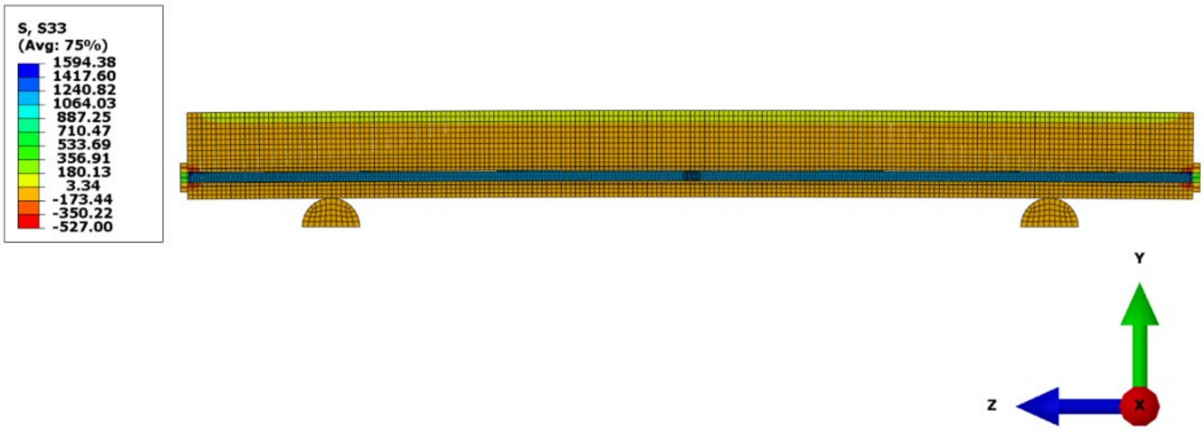

Fig. 10: Distribution of normal stresses S33 (global Z KS axis, perpendicular to the beam cross-section) along the beam axis as a result of post-tensioning.

With closer look at the normal stresses S33 distribution through the midspan beam cross-section shown in the left Figure 11 it is obvious that the compression stresses at lower beam surface is -84,42 MPa and at the upper beam surface is reaching 17,97 MPa. It is important to note that the level of post-tensioned force was limited to 300 kN to keep the tensile stresses at the top surface of the beam below 20 MPa, since there the tensile strength of the beam is limited to the tensile strength of the UV adhesive. At the same time the tensile stresses developed in the glass fiber tendon reached 1219,5 MPa which represent 66 % of the tensile strength obtained by the experimental analysis presented in previous chapter. Another important location for the normal stresses S33 distribution is contact area between the end steel plates and glass sheets around the hole, where the post-tensioning load is transferred from the glass fiber tendon to the glass sheets. In the right Figure 11 it is shown that the corresponding concentration compression stresses in glass sheets are of magnitude of around 527 MPa which is well below the corresponding nominal glass compression resistance of 1000 MPa. This level of compression stresses developed in glass elements is similar to the compression stresses obtained by other researchers (like in (Bedon & Louter, 2017) dealing with various post-tensioning laminated glass beams. However, these compressive stresses represent high stress concentrations on a relatively small area which can cause large differences in local deformations and potentially premature glass failure. Therefore, based on this numerical simulation we suggest to further explore and develop better contact steel plate for post-tensioning load transfer from glass fiber tendon to the glass sheets for more adequate contact compression stresses distribution at this location.

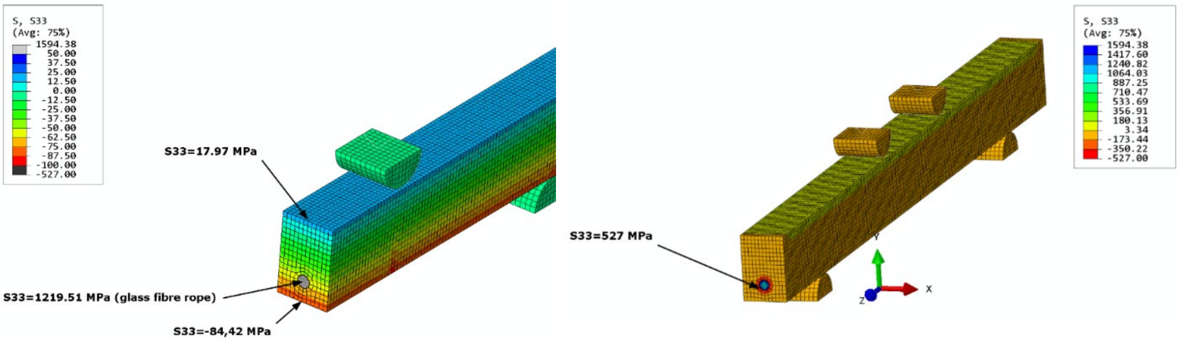

Fig. 11: Distribution of normal stresses S33 trough the mid-span beam cross-section (left) and concentrated normal stresses S33 at the location of contact between glass sheet and steel plate as a result of post-tensioning.

In the Figure 12 the vertical displacements U2 of studied beam are shown caused by the eccentrically positioned post-tensioning load application. As expected, and also in agreement with findings by other researchers ((Bedon & Louter, 2017), the uplifting at the midspan of the proposed beam can be observed and reached 1,64 mm.

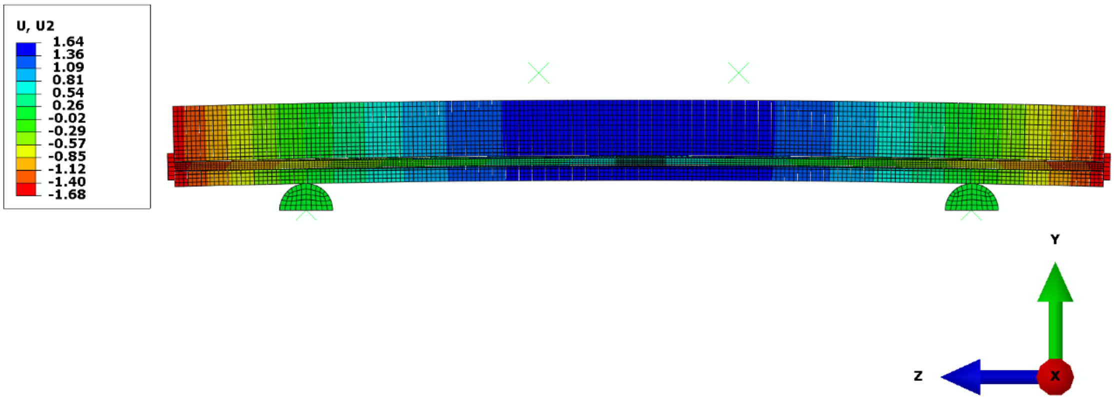

Fig. 12: Vertical displacements U2 [mm] (Y direction) of studied glass beam after post-tensioning.

The results for normal stresses S33 distribution along the whole beam for the second load step with the applied two vertical forces acting simultaneously with the post-tensioning force are presented in the Figure 13. The numerical simulation was performed up to a 250 kN of total applied vertical forces, whereas in the Figure 13, Figure 14, and Figure 15 the results are shown for the total vertical load of 118,65 kN only. At this vertical load level, the tensile normal stresses S33 (see Figure 14) at the bottom of mid-span cross-section reached the adhesive tensile load bearing capacity limit which was taken as 20 MPa for the purpose of the present study. At the top surface of mid-span cross section, the compressive stresses of 79,8 MPa were simulated and are well below the compression load bearing capacity of glass. The tensile stresses in glass fiber tendon increased from 1219,5 MPa to 1248 MPa which is 2,3% increase when vertical load is applied. In regards to the compression concentration stresses at the contact area between end transferring steel plates and flat glass around the hole the increase of up to 537,9 MPa is observed as shown in the right Figure 14.

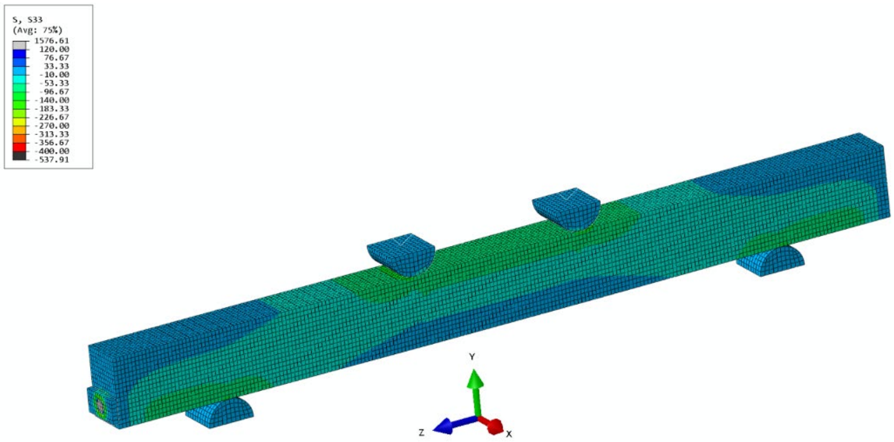

Fig. 13: Distribution of normal stresses S33 (global Z KS axis) along the beam axis as a result of simultaneously acting the post-tensioning and applied two vertical forces of 59,32 kN.

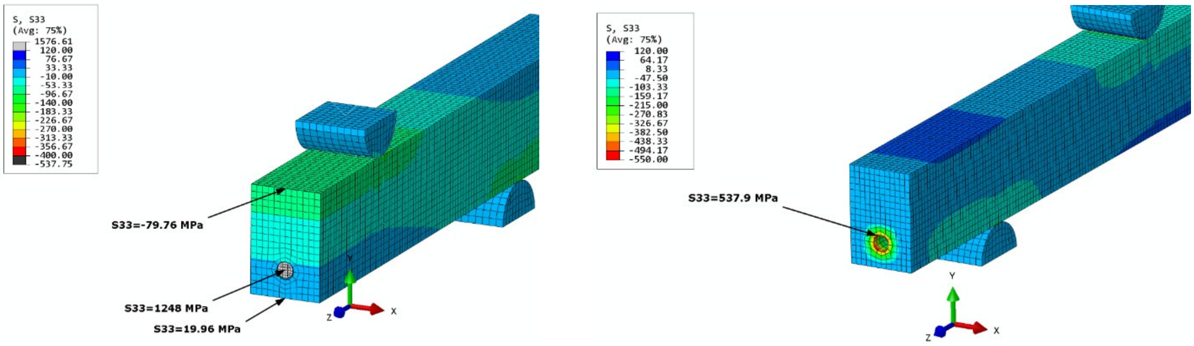

Fig. 14: Distribution of normal stresses S33 trough the mid-span beam cross-section (left) and concentrated normal stresses S33 at the location of contact between glass sheet and steel plate as a result of post-tensioning and applied two vertical forces of 59,32 kN.

The shear load bearing capacity and particularly the glass-to-glass adhesive interaction was one the main concern from the beginning of the present study and also the parameter governing the load bearing capacity of the beam. Therefore, the shear stresses S23 along the considered beam as a result of two vertical forces equal to 59,32 kN are presented in the Figure 15. It is shown that the shear stresses are below 17 MPa in the area where interlaminar shear stresses between adjacent glass sheets can emerge. To limit the contact shear stresses below this value was also the control parameter since the shear load bearing capacity of UV glue was considered as 17 MPa as stated by the adhesive producer.

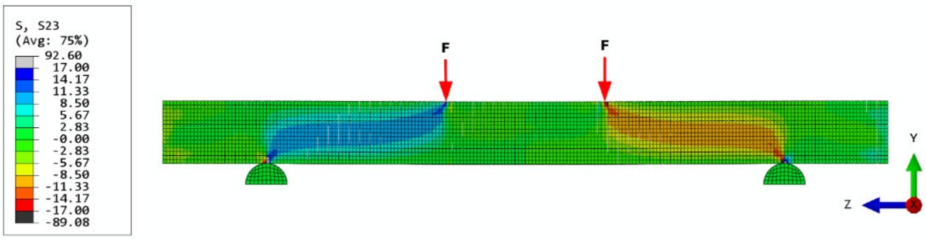

Fig. 15: Distribution of shear stresses S23 (global Y KS axis) along the beam axis as a result of applied two vertical forces of 59,32 kN.

Additionally, the total applied vertical force in a relationship to a corresponding mid-span deflection of the beam is shown in the Figure 16 up to the force of 247 kN. Dashed red line represents the load level and corresponding deflection at which the shear and tensile strength of UV glue in contact area between glass sheets is reached. It is also obvious that the force-displacement relationship is linear since the material characteristics are linear and the numerical model does not consider damage and cracking of the elements. Furthermore, the stiffness of the simulated post-tensioned glass beam reached high value of 36,62 kN/mm. The present numerical model should be upgraded in order to simulate failure mechanism and to evaluate the potential post-fracture behaviour and the corresponding ductility which can be limited in comparison to the glass beams with the steel reinforcement.

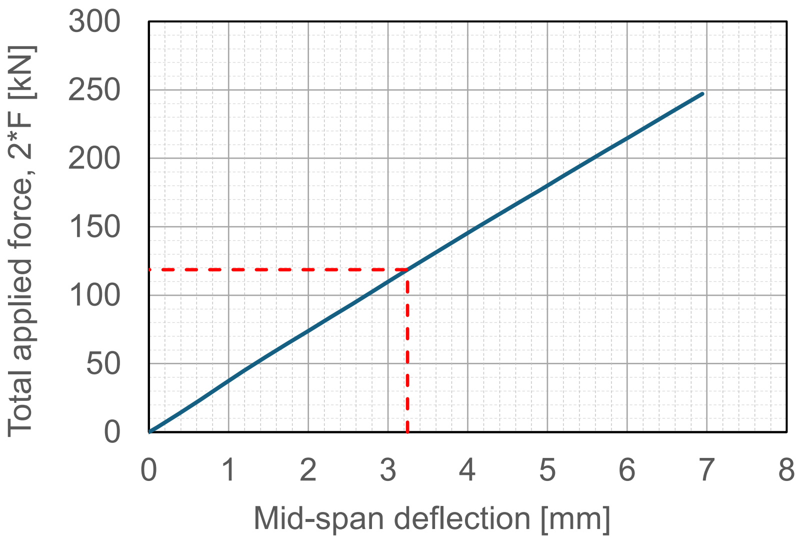

Fig. 16: Total applied vertical force versus corresponding mid-span vertical displacement relationship.

4. Conclusions

In the present study the specific concept of a four-point bending post-tensioned glass beam was studied with the aid of numerical simulation in ABAQUS software. The beam is assembled with the series of 70 annealed float glass sheets stacked together along the longitudinal axis of the beam which is oriented perpendicularly to the surfaces of the stacked glass sheets. At the bottom part of the beam cross-section the hole is provided for the placement of a glass fiber tendon running longitudinally trough the beam and is fixed at each end and followed by post-tensioning. To provide the connection between flat glass sheets we considered acrylate UV adhesive and EVA interlayer foil. Both of them were experimentally examined for the shear bonding behaviour with the specially designed shear specimens. Based on the experimental results we decided to use UV adhesive for further numerical simulation of the post-tensioned beam since it exhibits stiffer behaviour and it can be applied in a very thin layer and thus the contact area anomalies can be avoided. With the 3D finite element numerical model, the stresses distributions with the focus on critical areas and stress concentrations were studied and evaluated. Additionally, the load bearing capacity and stiffness of the proposed post-tensioned glass beam was simulated. The proposed beam geometry was considered with the present dimensions as there is the ambition to prepare the same physical model and conduct the experimental analysis in the laboratory.

Based on the numerical simulation of the proposed post-tensioned glass beam the following main conclusions can be drawn:

- Post-tensioning of the beam with the force of 300 kN can be applied
- High contact compressive concentration stresses appear at the contact between the end fixing steel plate and glass sheets in the area around the hole as a consequence of tensile post-tensioning load transfer from the glass fiber tendon to the attached steel plate. Since this is an early exploratory research of the proposed post-tensioning concept further research is suggested to design a different steel plate to provide more evenly distributed compressive contact stresses between the steel plate and glass sheets.
- For the considered geometry of the proposed pour-point bending post-tensioned glass beam the load bearing capacity of 118,65 kN was evaluated. At this load level the shear and tensile strength of UV adhesive in contact areas between glass sheets are reached. However, there are still reserves in the load bearing capacity of glass fiber rope and glass sheets.
- The proposed beam exhibited very stiff behaviour with the linear bending stiffness equal to 36,62 kN/mm. High stiffness behaviour can be attributed to post-tensioning and the geometry of the simulated beam.
- To confirm the presented numerical model and to check the potential post-fracture behaviour and ductility the experimental analysis of the proposed post-tensioned glass beam must be conducted in the laboratory.

Finally, the proposed post-tensioned glass beam shows a potential for further research to fully engage the high compressive strength of flat glass sheets and superior tensile strength of glass fiber tendons. Another option is to use a steel tendon for post-tensioning instead of glass fiber ropes. With the rising of the cast glass development and the possibility to produce larger specially designed glass elements with the enhanced surface levelness there is a high potential to assemble a high performance post-tensioned glass beam designed with concept presented and studied in this article.

Acknowledgements

The authors acknowledge the financial support from the Slovenian Research agency (research core funding No. P2-0185).

References

Aurik, M. (2017). Structural Aspects of an Arched Glass Masonry Bridge. http://repository.tudelft.nl/

Aurik, M., Snijder, A., Noteboom, C., Nijsse, R., & Louter, C. (2018). Experimental analysis on the glass-interlayer system in glass masonry arches. Glass Structures and Engineering, 3(2), 335–353. https://doi.org/10.1007/s40940-018-0068-7

Bedon, C., & Louter, C. (2017). Finite Element analysis of post-tensioned SG-laminated glass beams with adhesively bonded steel tendons. Composite Structures, 167, 238–250. https://doi.org/10.1016/j.compstruct.2017.01.086

Bedon, C., & Louter, C. (2018). Numerical investigation on structural glass beams with GFRP-embedded rods, including effects of pre-stress. Composite Structures, 184, 650–661. https://doi.org/10.1016/j.compstruct.2017.10.027

Bedon, C., & Louter, C. (2019). Structural glass beams with embedded GFRP, CFRP or steel reinforcement rods: Comparative experimental, analytical and numerical investigations. Journal of Building Engineering, 22, 227–241. https://doi.org/10.1016/j.jobe.2018.12.008

Bristogianni, T., Oikonomopoulou, F., Veer, F. A., Snijder, A., & Nijsse, R. (2017). Production and Testing of Kiln-cast Glass Components for an Interlocking, Dry-assembled Transparent Bridge.

Bristogianni, T., Oikonomopoulou, F., Veer, F., & Nijsse, R. (2021). Exploratory Study on the Fracture Resistance of Cast Glass. International Journal of Structural Glass and Advanced Materials Research, 5(1), 195–225. https://doi.org/10.3844/sgamrsp.2021.195.225

Cagnacci, E., Orlando, M., Salvatori, L., & Spinelli, P. (2021). Four-point bending tests on laminated glass beams reinforced with FRP bars adhesively bonded to the glass. Glass Structures and Engineering, 6(2), 211–232. https://doi.org/10.1007/s40940-021-00147-9

Dimas, M., Oikonomopoulou, F., & Bilow, M. (2022). IN BETWEEN: An Interlayer Material Study Towards Circular, Dry-Assembly, Interlocking Cast Glass Block Structures. Challenging Glass 8: Conference on Architectural and Structural Applications of Glass, CGC 2022. https://doi.org/10.47982/cgc.8.416

Louter, C., Belis, J., Veer, F., & Lebet, J. P. (2012). Structural response of SG-laminated reinforced glass beams; experimental investigations on the effects of glass type, reinforcement percentage and beam size. Engineering Structures, 36, 292–301. https://doi.org/10.1016/j.engstruct.2011.12.016

Louter, C., Leung, C., Kolstein, C., & Vambersky, H. (2010). Structural Glass Beams with Embedded Glass Fibre Reinforcement. 439–448. http://icom.epfl.ch/

Louter, C., Nielsen, J. H., & Belis, J. (2013). Exploratory experimental investigations on post-tensioned structural glass beams. In Structures and Architecture: New concepts, applications and challenges (pp. 358–365). CRC Press. https://doi.org/10.3233/fde-130012

Martens, K., Caspeele, R., & Belis, J. (2016). Development of Reinforced and Posttensioned Glass Beams: Review of Experimental Research. Journal of Structural Engineering, 142(5). https://doi.org/10.1061/(asce)st.1943-541x.0001453

Oikonomopoulou, F., Bristogianni, T., Barou, L., & Veer, F. (2018). Interlocking cast glass components, Exploring a demountable dry-assembly structural glass system. https://www.researchgate.net/publication/329917259

Properties of Adhesives at a glance. (2017). https://assets.bohle.com/image/upload/documents/Klebstoffeigenschaften_EN_uzcrzt

Silvestru, V. A., Deng, Z., Michels, J., & Taras, A. (2024). Structural behaviour of laminated glass beams reinforced and post-tensioned with adhesively bonded iron-based shape memory alloy tendons. Engineering Structures, 316. https://doi.org/10.1016/j.engstruct.2024.118494

Snijder, A., Aurik, M., Veer, F., Louter, C., & Nijsse, R. (2016). Modeling structural behaviour of a dry-assembled glass block bridge with soft PVC interlayer. Proceedings of the Sixth International Conference on Structural Engineering, Mechanics and Computation, 1–4.

Snijder A., Smits J., Bristogianni T., & Nijsse R. (2016). Design and Engineering of a Dry Assembled Glass Block Pedestrian Bridge: Vol. CGC 5.

Strato glass interlayers, data sheets for EVA interlayers. (2018). https://www.satinal.it/en/s-lab-documentation/

UV Adhesive Verfix LV 740, Technical data. (2017). https://assets.bohle.com/image/upload/documents/TD_LV740_TDLV74_wtsaz3